JOURNAL OF GEOPHYSICAL RESEARCH, VOL. 112, D13204, doi:10.1029/2006JD008267, 2007

3-D aerosol-cloud radiative interaction observed in collocated MODIS and ASTER images of cumulus cloud fields

Guoyong Wen,[1,2] Alexander Marshak,[1] Robert F. Cahalan,[1] Lorraine A. Remer,[1] and Richard G. Kleidman[3]

Received 15 November 2006; revised 8 January 2007; accepted 27 March 2007; published 6 July 2007.

[1] Three-dimensional (3-D) aerosol-cloud interaction is examined by analyzing two images containing cumulus clouds in biomass-burning regions in Brazil. The research consists of two parts. The first part focuses on identifying 3-D cloud impacts on reflectances for the pixels selected for the MODIS aerosol retrieval based purely on observations. The second part of the research combines the observations with radiative transfer computations to identify key parameters in the 3-D aerosol-cloud interaction. We find that 3-D cloud-induced enhancement depends on the optical properties of nearby clouds as well as on wavelength. The enhancement is too large to be ignored. Associated bias error in one-dimensional (1-D) aerosol optical thickness retrieval ranges from 50 to 140% depending on wavelength and the optical depth of nearby clouds, as well as aerosol optical thickness. We caution the community to be prudent when applying 1-D approximations in computing solar radiation in clear regions adjacent to clouds or when using traditional retrieved aerosol optical thickness in aerosol indirect effect research.

Citation: Wen, G., A. Marshak, R. F. Cahalan, L. A. Remer, and R. G. Kleidman (2007), 3-D aerosol-cloud radiative interaction observed in collocated MODIS and ASTER images of cumulus cloud fields, *J. Geophys. Res.*, *112*, D13204, doi:10.1029/2006JD008267.

1. Introduction

[2] Aerosols play a critical role in the process of cloud formation. A change in aerosol properties may directly impact atmospheric radiation and also lead to a change in the microphysical and radiative properties of clouds and thus directly and indirectly influence the Earth's climate. Analyzing AERONET [see *Holben et al.*, 1998] ground-based network data, *Kaufman and Koren* [2006] recently found that absorbing and nonabsorbing aerosols affect cloud cover differently. While absorbing aerosols prevent clouds from forming, nonabsorbing aerosols extend cloud life times and are associated with enhanced cloud cover. This complements the fundamental theory of *Twomey* [1977] that ties an increase of anthropogenic aerosol to possible consequences to global climate change. An example of an application of this theory is the modification of cloud properties through a change in cloud condensation nuclei (CCN) in ship tracks observed from space [*Platnick et al.*, 2000; *Coakley et al.*, 1987]. However, assessing and quantifying the indirect effect of aerosol on cloud properties and climate on global scale still remains a great challenge. The radiative forcing of aerosol indirect effect on climate has been identified as the most uncertain among other radiative forcing factors [*Intergovernmental Panel on Climate Change*, 2001]. For example, the effect of aerosols on cloud albedo has a large range of uncertainties estimated as cooling between -2 and 0 W/m^2. The level of scientific understanding of aerosol indirect effect is categorized as "very low." Global observation of aerosol and cloud properties from satellite is one way to advance our understanding of aerosol indirect effect on the Earth's climate and to reduce its uncertainties.

[3] However, aerosol and cloud properties inferred from satellite observations are subject to uncertainties. This is partly because cloud and aerosol properties are derived from the satellite-observed reflected solar radiation on the basis of various assumptions about the Earth's surface, atmosphere, aerosols, and clouds. For operational purpose, the atmosphere, aerosols, and clouds are usually assumed to be horizontally homogeneous and plane parallel, which is called the 1-D approximation or plane-parallel approximation (PPA). In this approximation, it is assumed that radiative properties of an individual pixel are independent of its neighbors. Many studies have shown that 3-D cloud structure has a complicated impact on the retrievals of cloud properties [e.g., *Chambers et al.*, 1997; *Várnai and Marshak*, 2002; *Iwabuchi and Hayasaka*, 2003; *Horváth and Davies*, 2004; *Marshak et al.*, 2006]. In this study, we focus on how 3-D cloud structure affects reflectance in the clear region near clouds and what are the consequences of this enhanced reflectance on aerosol retrievals.

[1]NASA Goddard Space Flight Center, Greenbelt, Maryland, USA.
[2]Goddard Earth Sciences and Technology Center, University of Maryland Baltimore County, Baltimore County, Maryland, USA.
[3]Science Systems and Applications, Inc., Lanham, Maryland, USA.

0148-0227/07/2006JD008267$09.00

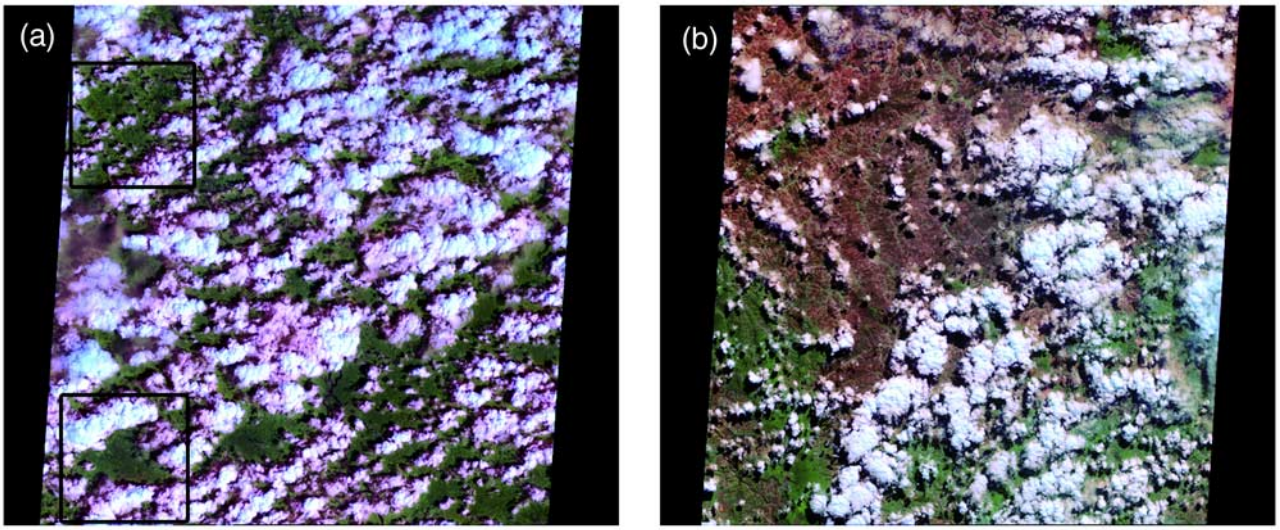

Figure 1. (a) ASTER image of scene 1 centered at (0°N, 53.78°W) acquired on 25 January 2003. (b) ASTER image of scene 2 centered at (17.1°S, 42.16°W) acquired on 9 August 2001. Two black boxes in Figure 1a show the regions for detail analysis. The solar zenith angle is 32° and 41° for Figures 1a and 1b, respectively. RGB = (2.1, 0.86, 0.55 μm) for both images.

[4] Aerosol optical thickness (AOT) in the clear region near clouds is a key parameter in the study of aerosol indirect effect from remote-sensing instruments. In this region the atmosphere experiences a big change in optical properties with optically thick clouds surrounded by optically thin aerosols. Since clouds, aerosols, and molecules all scatter sunlight at wavelengths selected for aerosol retrievals, 3-D aerosol-cloud radiative interactions have a large impact on clear region reflectance and thus on associated aerosol retrievals. As we demonstrate in this paper, the conventional 1-D retrieval can lead to a large bias in aerosol optical depth. Thus, to understand 3-D aerosol-cloud radiative interaction, to quantify its impact on aerosol retrievals is important to reduce uncertainties in estimates of aerosol indirect effects on the Earth's climate using satellite observations.

[5] 3-D aerosol-cloud radiative interactions have received increasing attention in the past several years. Efforts were made to parameterize 3-D cloud effects on reflectance in clear regions of Landsat ETM+ images [*Wen et al.*, 2001; *Nikolaeva et al.*, 2005]. 3-D radiative transfer models were used to compute 3-D cloud effects near ideal clouds (infinitely long cuboidal bar cloud, 3-D cubic cloud, horizontally semi-infinite cloud) [*Kobayashi et al.*, 2000; *Cahalan et al.*, 2001; *Nikolaeva et al.*, 2005]. Using MODIS 1-km resolution cloud optical depth product, and the brightness temperature at 11 μm to construct a realistic 3-D cloud field, *Wen et al.* [2006] demonstrated that a 3-D cloud has a strong impact on the reflected clear-sky solar radiation and thus on associated 1-D aerosol retrieval.

[6] This work is an extension of our previous research. It includes the (1) analysis of MODIS aerosol retrievals for possible 3-D cloud effects, (2) computation of 3-D cloud effects at 0.5-km resolution and examination of 3-D cloud effects on pixels selected by MODIS aerosol retrieval algorithm, and (3) study of 3-D cloud effects at a higher resolution not resolved by MODIS. The study is conducted for two cumulus cloud fields in Brazil. These two cloud fields are distinctive in terms of ''large'' and ''small'' aerosol loadings from MODIS retrievals to represent ''polluted'' and ''pristine'' scenes, respectively.

[7] The data sets are described in section 2 followed by data analyses in section 3. Section 4 presents 3-D cloud radiative effects computed in cloud fields. In the final section the results are summarized and discussed.

2. Data Description

[8] Two MODIS nadir-viewed scenes from the Terra satellite in biomass-burning regions of Brazil were acquired on 25 January 2003 (scene 1) and 9 August 2001 (scene 2). The size of both scenes is 80 $\times$ 68 km. These scenes entirely cover the collocated high-resolution Advanced Spaceborne Thermal Emission and Reflection Radiometer (ASTER) images of size $\sim$60 $\times$ 60 km [*Yamaguchi et al.*, 1998]. Scene 1, used earlier by *Wen et al.* [2006], is centered

Table 1. Information About the Two Scenes With Solar Zenith Angle (SZA), Solar Azimuth Angle (SAZ), Cloud Cover, Cloud Optical Depth (COD) With the Average (τ) Followed by the Standard Deviation (σ)

	Date Acquired	Center (lat,long)	SZA	SAZ	Cloud Cover, %	COD
Scene 1	25 January 2003	(0°N, 53.78°W)	32°	129°	53	τ = 12, σ = 10
Scene 2	9 August 2001	(17.1°S, 42.16°W)	41°	38°	40	τ = 8, σ = 8

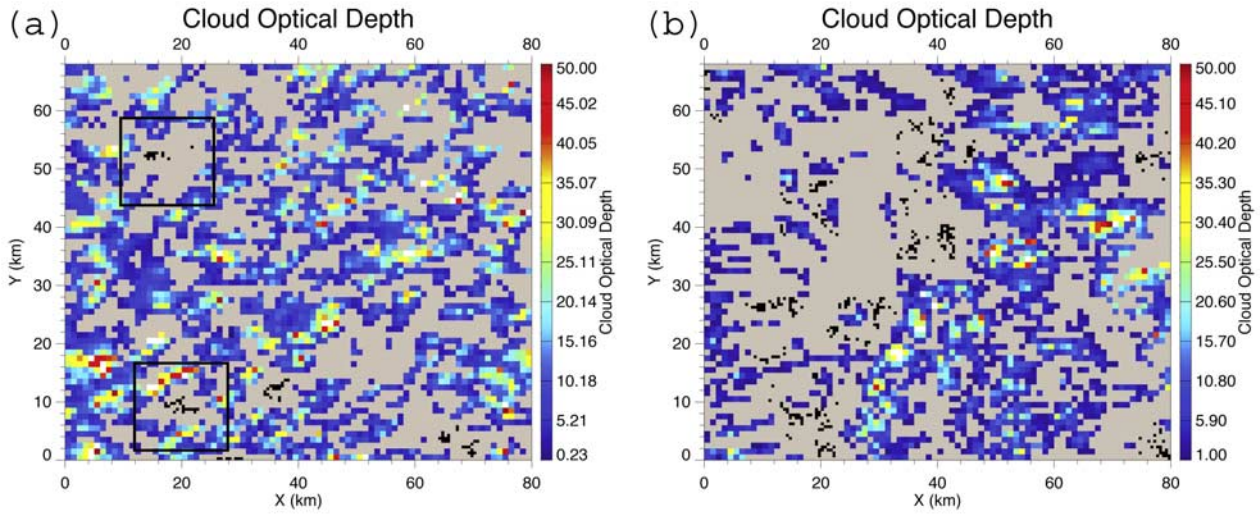

Figure 2. MODIS cloud optical depth fields for collocated ASTER images in Figures 1a and 1b for scene 1 and for scene 2, respectively. The average cloud optical depth and standard deviation are (a) τ (scene 1) $\sim$12 and σ (scene 1) $\sim$10 and (b) τ (scene 2) $\sim$8 and σ (scene 2) $\sim$8. The cloud cover is $\sim$53 and $\sim$40% for Figures 2a and 2b, respectively. Two squares outlined in black in Figure 2a show the regions for detail analysis. The small black points indicate the 500-m pixels from which the MODIS aerosol products were retrieved.

at the equator at 53.78° west, with a solar zenith angle (SZA) of 32° and a solar azimuth angle (SAZ) of 129° from north. Scene 2, used earlier by *Marshak et al.* [2006], is centered at 17.1° south and 42.16° west with a solar zenith angle of 41° and a solar azimuth angle of 38° from north. The two ASTER images are presented in Figure 1, and their characteristics are described in Table 1.

[9] The collection 4 of 1-km MODIS-retrieved cloud optical depth fields [*Platnick et al.*, 2003] of the two scenes are presented in Figure 2. Cloud fractions in scene 1 and scene 2 are 53 and 40%, with average cloud optical depth about 12 and 8, respectively. The MODIS surface albedo [*Moody et al.*, 2005] is used in this study. The surface in scene 1 is darker and more homogeneously covered by vegetation as compared to scene 2. The average surface albedo and associated standard deviation for the two visible bands at 0.47 and 0.66 μm and the mid-IR band at 2.13 μm are presented in Table 2. Scene 1 appears to be "polluted" with MODIS-retrieved average aerosol optical thickness of 0.37 at 0.47 μm and 0.19 at 0.66 μm. Aerosol loading in the "pristine" scene 2 is considerably smaller with an average aerosol optical thickness of $\sim$0.09 and $\sim$0.07 at 0.47 and 0.66 μm, respectively.

[10] Similar to the study conducted by *Wen et al.* [2006], the cloud top height is estimated using the brightness temperature at 11 μm using MODIS band 31; the vertical extinction profile is obtained assuming a linear distribution of cloud liquid water. To be consistent with a resolution of 0.5 km used in the MODIS aerosol retrieval algorithm [*Remer et al.*, 2005], a 1 $\times$ 1-km resolution pixel is split into four 0.5 $\times$ 0.5-km resolution pixels both for atmosphere products and the surface albedo to compute the 3-D cloud effects on the reflected solar radiation at 0.47 and 0.66 μm of the MODIS band 3 and band 1, respectively.

[11] We further examine the 3-D cloud effects at a smaller scale not resolved by MODIS. This is motivated by the fact that both cloud optical depth and MODIS-retrieved aerosol optical thickness have large spatial variability (Figures 2 and 3). It appears that cloud optical depth and aerosol amount from MODIS are related. Two regions of scene 1 indicated by the upper and lower boxes in Figure 2 are particularly interesting. The lower box has a clear region with a relatively large aerosol amount from MODIS (AOT $\sim$0.4) surrounded by optically thick clouds with an average optical depth of $\sim$14. In the upper box, the clear regions with relatively less aerosol loading from MODIS (AOT$\sim$0.3) are next to puffy cumulus with average optical depth of $\sim$7. In this work we retrieve cloud optical depth using 15-m resolution ASTER band 2 (0.66 μm) reflectance and estimate cloud top height using 90-m resolution ASTER brightness temperature at band 14 (11 μm). With the same aerosol properties as those for 0.5-km resolution,

Table 2. Average (α) and Associated Standard Deviation (σ) of Surface Albedo of Visible and Mid-IR Bands for Scene 1 and Scene 2, Estimated From *Moody et al.* [2005]

	0.47 μm	0.65 μm	2.13 μm
Scene 1	α = 0.011, σ = 0.003	α = 0.025, σ = 0.004	α = 0.055, σ = 0.006
Scene 2	α = 0.039, σ = 0.009	α = 0.079, σ = 0.018	α = 0.163, σ = 0.035

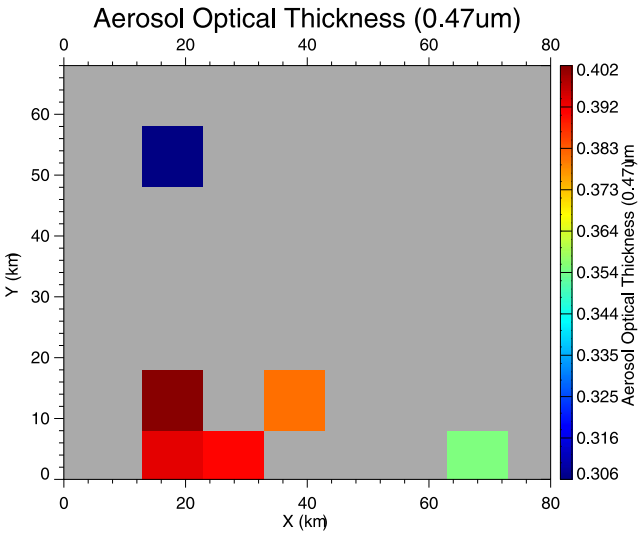

Figure 3. MODIS-retrieved aerosol optical thickness for scene 1 in Figure 2a. Aerosol optical thickness of ~0.4 near optically thick clouds (lower box in Figure 2a) is evidently larger than optical thickness (~0.3) near optically thin clouds (upper box in Figure 2a).

we perform radiative computation at 90-m resolution to investigate the 3-D effects at a scale not resolved by MODIS.

3. Analyses of MODIS Aerosol Retrieval

[12] Aerosol optical thickness is operationally retrieved at 0.47 and 0.66 μm, MODIS band 3 and band 1, respectively. The collection 4 MODIS aerosol product is used in this study. Details about the MODIS aerosol retrieval algorithm over land can be found in the work of *Remer et al.* [2005]. Here we highlight only several important steps of the retrieval algorithm needed to understand the effect of broken cumulus clouds on the retrieval of aerosol optical thickness. After applying the "cloud mask" procedure [*Martins et al.*, 2002] and rejecting 0.5 × 0.5-km pixels with relatively bright surfaces (at 2.1 μm), out of the remaining pixels in each 10 × 10-km area, we further reject 50% of the brightest and 20% of the darkest pixels. Note that the rejected pixels at 0.47- and 0.66-μm wavelength are not necessarily identical. If the number of surviving 0.5 × 0.5-km pixels in a 10 × 10-km area is larger than a threshold value (12 pixels in the current algorithm), their reflectance values are averaged and the aerosol optical thickness assigned to this 10 × 10-km area is retrieved. In this section we will focus only on those 0.5 × 0.5-km pixels that survived rejection and thus have been selected to contribute to aerosol retrievals.

[13] In Figure 2, the selected for aerosol retrieval pixels are indicated as black. It is evident that the "polluted" scene 1 has much fewer pixels selected for aerosol retrieval compared to the "pristine" scene 2, namely, 82 pixels selected for scene 1 versus 340 selected pixels for scene 2. Since the cloud fraction is ~53% for scene 1 and ~40% for scene 2 and each scene contains 160 × 136 pixels, only ~0.8 and ~2.6% of noncloudy pixels are selected for aerosol retrieval for the two scenes, respectively.

[14] The selected pixels are not uniformly distributed in space. In order to quantify the 3-D cloud effects, we need to examine the distributions of the selected pixels, their average reflectance, and associated standard deviation as a function of the distance to the nearest cloud. Figure 4 shows that the distance between the selected clear pixels and the nearest cloudy pixels ranges from 0.5 to 3.6 km

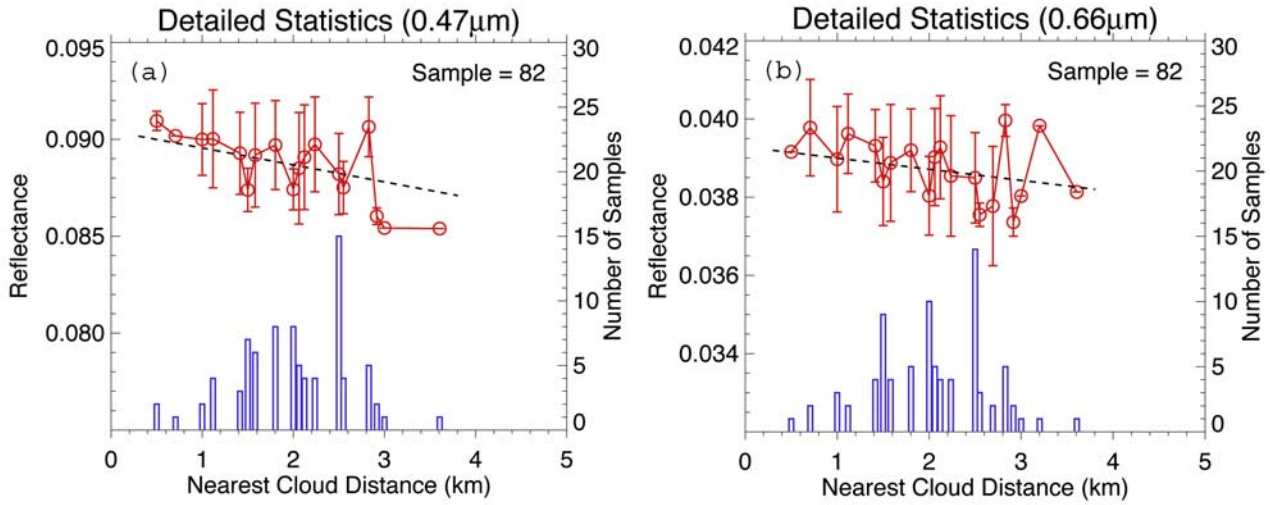

Figure 4. Averaged reflectance (circle, left scale) and standard deviation (vertical brackets, left scale) for pixels for aerosol retrieval for wavelength (a) 0.47 μm and (b) 0.66 μm of scene 1. Vertical bars show the distribution of those selected pixels (right scale) as a function of the nearest cloud distance. The average of the nearest cloud distance is ~2 km with a standard deviation of ~0.6 km. The slope of the best linear fit is about −0.0009/km at 0.47 μm and −0.0003/km at 0.66 μm. The average surface albedos and standard deviations are (a) $\alpha_{0.47\mu m} = 0.011$, $\sigma_{0.47\mu m} = 0.003$ and (b) $\alpha_{0.66\mu m} = 0.025$, $\sigma_{0.66\mu m} = 0.004$.

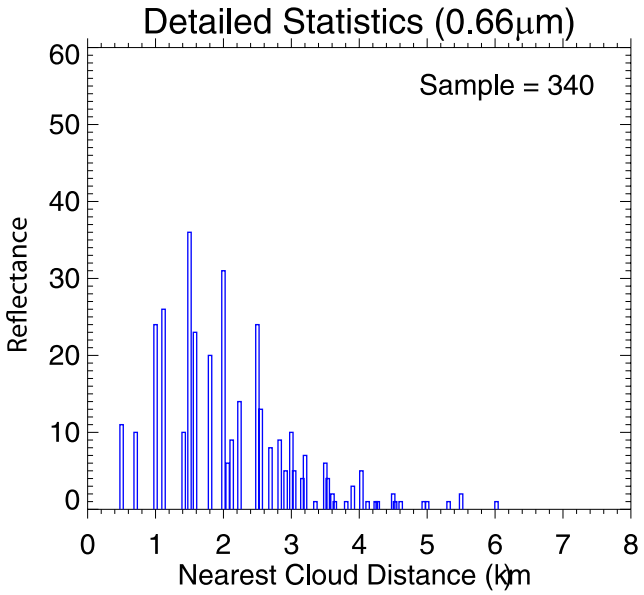

Figure 5. Distribution of selected pixels as a function of the nearest cloud distance at 0.66-μm wavelength for scene 2. The average of the nearest cloud distance is $\sim$2.15 km with a standard deviation of $\sim$0.97 km. The average surface albedos and standard deviations are $\alpha_{0.47\mu m} = 0.039$, $\sigma_{0.47\mu m} = 0.009$ and $\alpha_{0.66\mu m} = 0.079$, $\sigma_{0.66\mu m} = 0.018$.

with an average of 2 km and standard deviation of 0.6 km. Clouds were designated by the standard MODIS cloud mask algorithm [*Ackerman et al.*, 1998] and were used to retrieve cloud microphysical properties in collection 4 [*Platnick et al.*, 2003; Platnick, personal communication, 2006]. Note that these are separate cloud identification schemes compared to the one used internally by the MODIS aerosol algorithm [*Remer et al.*, 2005; *Martins et al.*, 2002]. There is no reason why an aerosol retrieval pixel could not coincide with a pixel identified as cloud by the cloud mask algorithms. The distribution shows that no aerosol pixels overlap with a cloud pixel and only three pixels are contiguous to clouds. With 6 pixels falling within 1 km of a cloud and 3 pixels lying beyond 3 km from cloud edges, about 90% of selected pixels are at a distance between 1 and 3 km from the nearest cloud edges. Note that the distributions of the population of selected clear pixels at the two bands are similar even though the selected clear pixels for the two bands are not necessarily the same.

[15] For scene 1 (the "polluted" image), the reflectance from the selected pixels decreases as a function of the distance to the nearest cloud. The rate of decrease of reflectance as determined by the best linear fit is -0.0009/km for 0.47 μm and -0.0003/km for 0.66 μm. Since the surface is dark and homogeneous, it is very unlikely that the decrease in the reflectance is due to the variability in the surface reflective properties. Also, a detailed examination with high-resolution ASTER image (section 5) shows no evidence for subpixel cloud contamination, in which the algorithm's cloud mask fails to identify a clearly identifiable cloud. Therefore the decrease in reflectance as a function of the distance to the nearest cloud is very likely due to 3-D radiative interaction.

[16] The surface reflectance of scene 2 (the "pristine" image) is more complicated. The surface is much brighter and more inhomogeneous compared to scene 1. The surface albedo is 0.04, 0.08, and 0.16 with standard deviations of 0.01, 0.02, and 0.04 for 0.47, 0.66, and 2.13 μm bands, respectively. The variability of surface albedo for this scene is so large that a 3-D radiative signature of the dependence of the clear-sky reflectance on the distance from cloud edges is not detectable. Thus only the distribution of the selected pixels for aerosol retrieval is presented below.

[17] Figure 5 shows the distribution of 340 selected clear pixels for aerosol retrieval for scene 2. The average distance between the selected clear-sky pixels to the nearest cloud is $\sim$2.15 km, which is very close to that in scene 1. The distribution of the nearest cloud distances for scene 2 is broader compared to scene 1 with a long tail extended to 6 km. The standard deviation of the distribution is $\sim$0.97 km for scene 2 versus $\sim$0.6 km for scene 1. In contrast to scene 1, 21 pixels contiguous to clouds as identified by the cloud algorithm were selected for aerosol retrieval. As for scene 1, a detailed examination of the selected clear pixels with the high-resolution ASTER image found no evidence of subpixel cloud contamination of those pixels.

4. 3-D Cloud Effects at the 0.5-km Resolution

[18] An I3RC (Intercomparison of 3D Radiation Codes) [*Cahalan et al.*, 2005] certified Monte Carlo (MC) code for radiative transfer in a 3-D cloudy atmosphere [*Marshak and Davis*, 2005] is used in this study. In contrast to the work of *Wen et al.* [2006] that computed the reflected solar radiation for scene 1 at the 1-km resolution, this section will discuss the radiation fields computed at the instrument resolution of 0.5 km for MODIS aerosol retrieval for both scene 1 and scene 2. We will further examine the details of the 3-D cloud effects at the 90-m resolution not resolved by MODIS in section 5.

[19] Similar to the work of *Wen et al.* [2006], the 1-km MODIS cloud optical depth is used with cloud top height estimated from brightness temperature at 11 μm of MODIS band 31 on Terra for both scenes. Other cloud structure assumptions are the following: Cloud base is assumed to be constant at 1 km and cloud liquid water vertical profile is assumed to be linear. Single-scattering properties of clouds such as the phase function and single-scattering albedo at two MODIS bands are computed assuming a gamma distribution of cloud droplet with an effective radius of 10 μm and effective variance of 0.1 [*Hansen*, 1971].

[20] Aerosol particles are assumed to have a lognormal size distribution with a standard deviation of 0.6 and modal radius of 0.13 μm and a single-scattering albedo of 0.9 [*Remer et al.*, 2005; *Reid et al.*, 1998]. For scene 1, the aerosol optical thickness is assumed to be 0.2 at 0.47 μm and 0.1 at 0.66 μm. For scene 2, the aerosol optical thickness is assumed to be 0.07 at 0.47 μm and 0.05 at 0.66 μm. For simplicity, the aerosols are assumed to be uniformly distributed in the following two layers: in a boundary layer below 2 km and in a free troposphere above 2 km. The aerosol optical thickness in the free troposphere

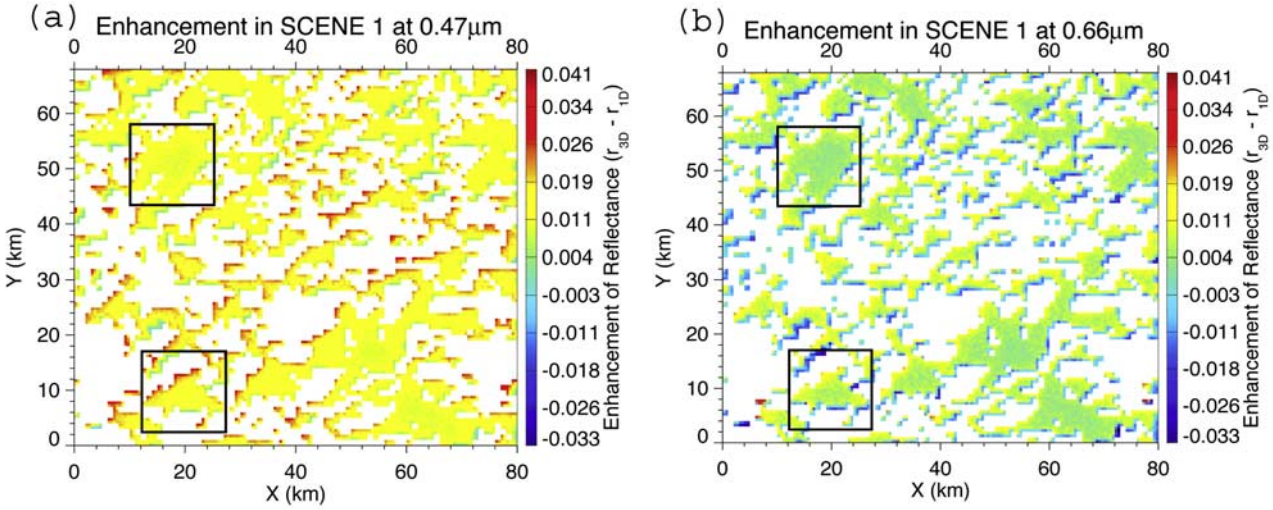

Figure 6. (a) Enhancement of reflected solar radiation due to 3-D effects for clear regions in the cumulus field for 0.47 μm and (b) for 0.66 μm. The direction of the incident solar radiation is toward the southeast with a solar azimuth angle of 129° defined from the north (clockwise). Cloud pixels are masked as white. The averages and associated standard deviations of the enhancement are (a) $\overline{\Delta r}_{0.47\mu m} = 0.015$ and $\sigma_{0.47\mu m} = 0.005$ and (b) $\overline{\Delta r}_{0.66\mu m} = 0.004$ and $\sigma_{0.66\mu m} = 0.008$. Two squares outlined in black show the regions for detail analysis.

is assumed to be 0.01 with all the rest of the aerosols in the boundary layer.

[21] Surface albedo fields from MODIS products [*Moody et al.*, 2005] are used in both scenes. The 1-km resolution MODIS-derived cloud optical properties and surface albedo are split into 0.5-km resolution pixels to compute the reflectance at the two bands for the MODIS aerosol retrievals. With the cloud optical depth field, aerosol and molecular properties, and boundary conditions adequately specified, the MC code computes reflectance r_{3D} over a cumulus cloud field. Without clouds, for the same aerosol and molecular properties, and surface albedo, the MC code also computes reflectance r_{1D}. The 3-D cloud effect or the enhancement is defined as the reflectance difference between the "true" value r_{3D} and its 1-D counterpart r_{1D}.

4.1. 3-D Cloud Effects for Scene 1

[22] Figure 6 illustrates the enhancement of reflectance in clear regions due to 3-D aerosol-cloud radiative interaction for scene 1. It is evident that clouds enhance reflected solar radiation almost everywhere except in shadowed pixels [see also *Nikolaeva et al.*, 2005]. It is seen that clouds have a stronger impact on the average enhancement of reflectance with less variability (the range and standard deviation) at the shorter wavelength compared to the longer wavelength (Figure 6).

[23] Spatial distributions of enhancement for the two wavelengths are similar with strong enhancement in front of the sunlit side of clouds and less enhancement (if any) for shadowed pixels. Away from cloud edges, the enhancement is relatively stronger near optically thick clouds (for example, the lower box in Figure 2a) than that near optically thin clouds (for example, the upper box in Figure 2a) for both wavelengths. One should note that shadowing reduces reflectance for wavelength at 0.66 μm resulting in negative enhancement. At 0.47 μm, however, even though enhancement is small over the shadowed pixel, the cloud-induced enhancement of reflectance is positive almost everywhere except for a few isolated shadowed pixels. This is because the surface at 0.47 μm is darker than that at 0.66 μm with surface albedo of ~0.01 versus ~0.025, respectively, and the 1-D clear-sky reflectance at 0.47 μm is less sensitive to the surface albedo than that at 0.66 μm. One can demonstrate that the 1-D clear-sky reflectance is approximately a linear function of surface albedo [e.g., *Wen et al.*, 1999, equation (8)]. The surface contribution to the 1-D reflectance approximately equals to the two-way transmission multiplied by the surface albedo. Thus the 1-D reflectance at 0.47 μm with smaller transmittance is less sensitive to surface albedo compared to that at a longer wavelength of 0.66 μm. When sunlight is blocked by a cloud, the shadowing effects are expected to be larger over a bright surface for a longer wavelength than that over a dark surface for a shorter wavelength. For scene 2 with larger surface albedo at both wavelengths, surface-cloud interaction leads to a reduction of reflectance over shadowed pixels as shown in the next subsection. Still, with larger surface albedo at 0.66 μm, the shadowing effect leads to larger reduction at longer wavelength of 0.66 μm compared to shorter wavelength at 0.47 μm.

[24] The radiative effects of clouds on the reflectance in clear regions can be quantified by the statistics of the enhancement and spatial distribution of noncloudy pixels in terms of nearest cloud distance similar to the work of *Wen et al.* [2006]. The statistics of the enhancement for all noncloudy pixels as well as those selected for MODIS aerosol retrieval are presented in Figure 7 for the two wavelengths. For all noncloudy pixels, as presented in Figures 7a and 7c, a common feature of the distribution is the large variability of the enhancement within ~1 km from

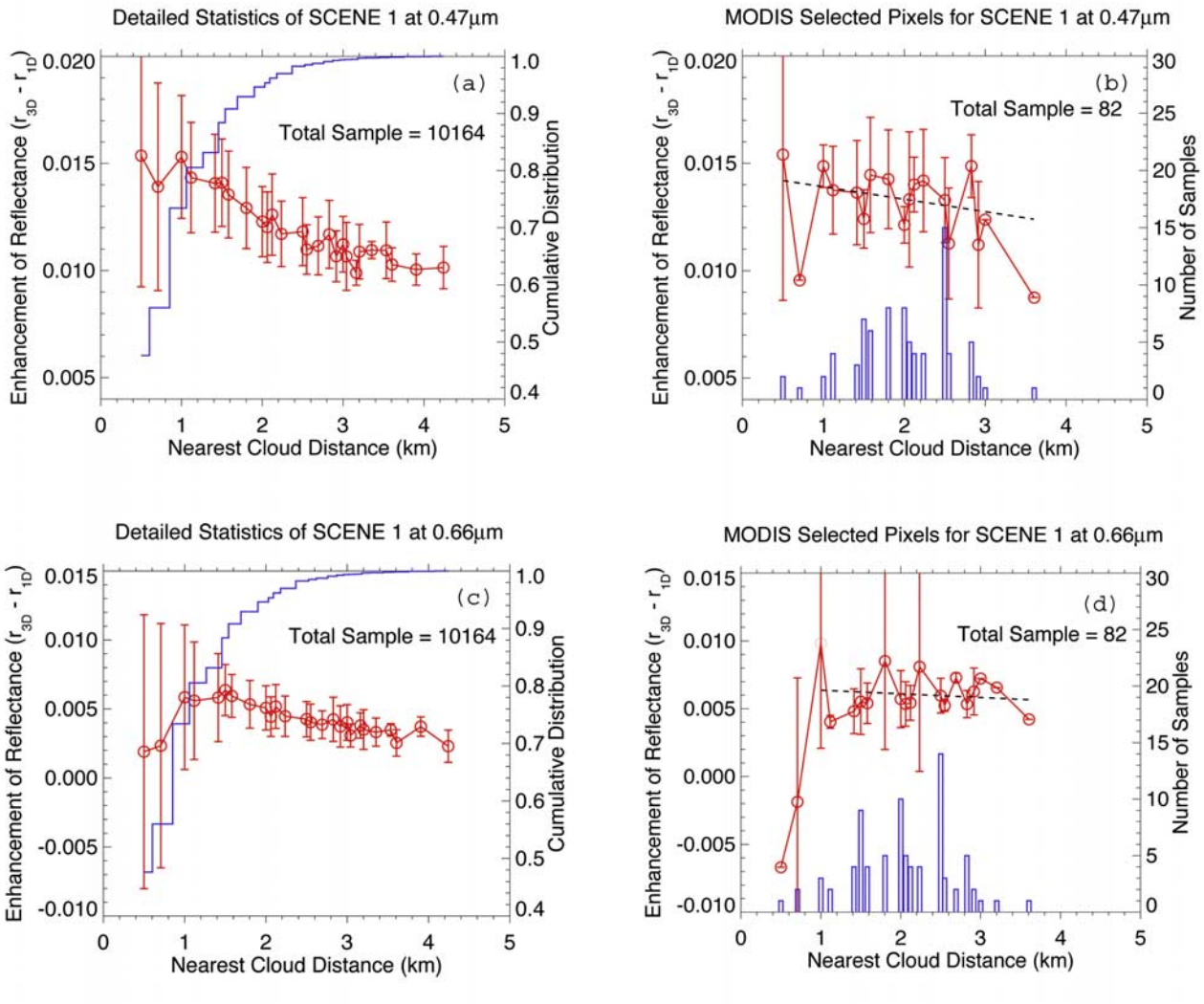

Figure 7. Average enhancement (circles, left scale) and standard deviation (vertical brackets) for clear pixels as a function of the nearest cloud distance. Cumulative and sample distributions of clear pixels as a function of the nearest cloud distance (right scale) for scene 1. Results are presented in Figures 7a and 7c for all noncloudy pixels at wavelengths 0.47 and 0.66 μm, respectively. Results for MODIS-selected pixels are presented in Figures 7b and 7d, respectively. The slope of the best linear fit for the MODIS pixels is about -0.0006/km and -0.0003/km for wavelengths 0.47 and 0.66 μm, respectively. Outliers with nearest cloud distance of 0.5 and 0.7 km are excluded in computing the slope for 0.66 μm.

clouds for both wavelengths. In this cloud neighboring area, the large variability is associated with less enhancement or reduction over the shadowed pixels and strong enhancement near the sunlit side of clouds. The average enhancement and associated variability decrease with the nearest cloud distance for both wavelengths around 1 km away from cloud edges. The enhancement reaches an asymptotic value of about 0.01 at 0.47 μm and 0.004 at 0.66 μm about 3 km away from clouds. It can be shown [e.g., *Wen et al.*, 1999] that, in 1-D retrieval, the 3-D cloud-induced enhancement of 0.01 and 0.004 leads to an overestimation of the aerosol optical thickness of about 0.1 and 0.04 for the two wavelengths, respectively. Compared with the true aerosol optical thickness of 0.2 and 0.1 at the two wavelengths, the aerosol optical thickness retrieval from a 1-D model results in 50 and 40% bias errors, respectively.

[25] It is interesting to examine the statistics of the enhancement for pixels selected by the MODIS aerosol algorithm (Figures 7b and 7d). The enhancement of the MODIS pixels resembles closely the enhancement to the pixels in the larger data set, although the enhancement of the MODIS pixels beyond the 2-km mark is slightly higher ($\sim$0.001 to 0.002) than in the general data set, meaning that the selection process in the MODIS algorithm does not shield the final product from artificial 3-D enhancement. The enhancement for MODIS-selected pixels has a decreasing trend with the nearest cloud distance for both wavelengths. The trends of the enhancement are very

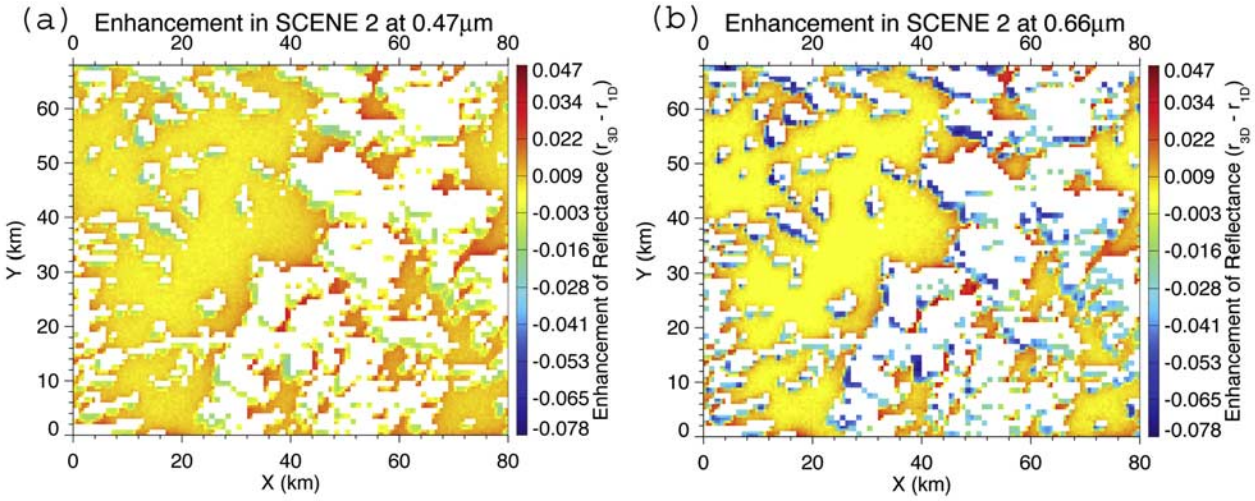

Figure 8. Enhancement of reflected solar radiation due to 3-D effects for clear regions in a cumulus field for scene 2 (a) for 0.47 μm and (b) for 0.66 μm. The direction of incident solar radiation is from the northeast with a solar azimuth angle of 38° from north (clockwise). Pixels identified as clouds from the MODIS cloud algorithms are masked as white. The averages and associated standard deviations of the enhancement are $\overline{\Delta r}_{0.47\,\mu\mathrm{m}} = 0.006$ and $\sigma_{0.47\,\mu\mathrm{m}} = 0.008$, and $\overline{\Delta r}_{0.66\,\mu\mathrm{m}} = -0.003$ and $\sigma_{0.66\,\mu\mathrm{m}} = 0.02$, for (a) and (b), respectively.

similar to those for reflectance at the two wavelengths in section 3.

[26] For all noncloudy pixels, there is a distinguishable difference in the distributions of the enhancement near cloud edges between the two wavelengths. At 0.66 μm, starting at the nearest cloud distance of 0.5 km, just next to clouds, the average enhancement increases from 0.002 and reaches a maximum of 0.006 at 1 km away from clouds then decreases with the distance from the cloud edges (Figure 7c). At 0.47 μm, the average enhancement almost monotonically decreases reaching an asymptotic value about 0.01 at a distance about 3 km away from clouds (Figure 7a). Again, this difference is primarily due to much stronger reduction over shadowed pixels at 0.66 μm compared to that at 0.47 μm. The variability in the enhancement measured by the standard deviation for 0.66 μm is about twice as large as that for 0.47 μm in the cloud neighboring area (0.5–1 km) (Figures 7a and 7c).

[27] The cumulative distribution of all noncloudy pixels demonstrates that the population of clear pixels decreases rapidly as a function of nearest cloud distance (Figure 7a). Ninety percent of all clear pixels are within a range of about 1.6 km from cloud edges. Only about 5% of clear pixels are more than 2 km beyond from cloud edges. At a distance of 3 km away from cloud edges, there are less than 1% of clear pixels left. Sharp reduction of the number of clear pixels with the distance from cloud edges for cumulus clouds were also reported by *Joseph and Cahalan* [1990] from the Landsat data and by *Lane et al.* [2002] from the ground-based measurements.

[28] It is also interesting to note that, in this study, using 0.5-km resolution data, the cloud neighboring region, a 1-km-wide band contiguous to the cloud edges, is narrower than that from the 1-km resolution data used in the work of *Wen et al.* [2006]. The apparent wider cloud neighboring area at 1-km resolution image is primarily due to a coarse resolution used in that study. At a resolution coarser than the true shadow size, the entire pixel would be a shadowed pixel even if it were partly shadowed. Thus it is necessary to study 3-D aerosol-cloud interaction in a finer scale.

4.2. 3-D Cloud Effects for Scene 2

[29] Figure 8 shows images of 3-D cloud effects for the "pristine" scene 2. Aerosol optical thickness is assumed to be 0.07 at 0.47 μm and 0.05 at 0.66 μm, slightly less than that from MODIS retrieval at the two wavelengths. Similar to the "polluted" scene 1, clouds enhance the reflected solar radiation almost everywhere except for the shadowed pixels for both wavelengths. From cloud shadows, we can see that the Sun is shining from the northeast when Terra was passing over the scene at about 10:30 am in local time on 9 August 2001 in the Southern Hemisphere.

[30] Clouds in scene 2 have a different pattern compared to scene 1. Clouds are mostly in the right part of the image with small scattered cumuli on the left. The enhancement in clear gaps on the right part of the image is evidently larger than that on the left part. The shadowing reduction and sunlit enhancement can be clearly identified.

[31] Similar to scene 1, 3-D clouds have stronger impact on the average enhancement of reflectance with less variability (the range and standard deviation) at the shorter wavelength compared to the longer wavelength (Figure 8). It is interesting to note that, at 0.66 μm, the average enhancement (reduction!) for all noncloudy pixels is negative (−0.003) with a large standard deviation of 0.02. One can see that, away from the clouds, in the cloud-free area on the left side of the image, 3-D clouds-induced enhancement appears to be uniform.

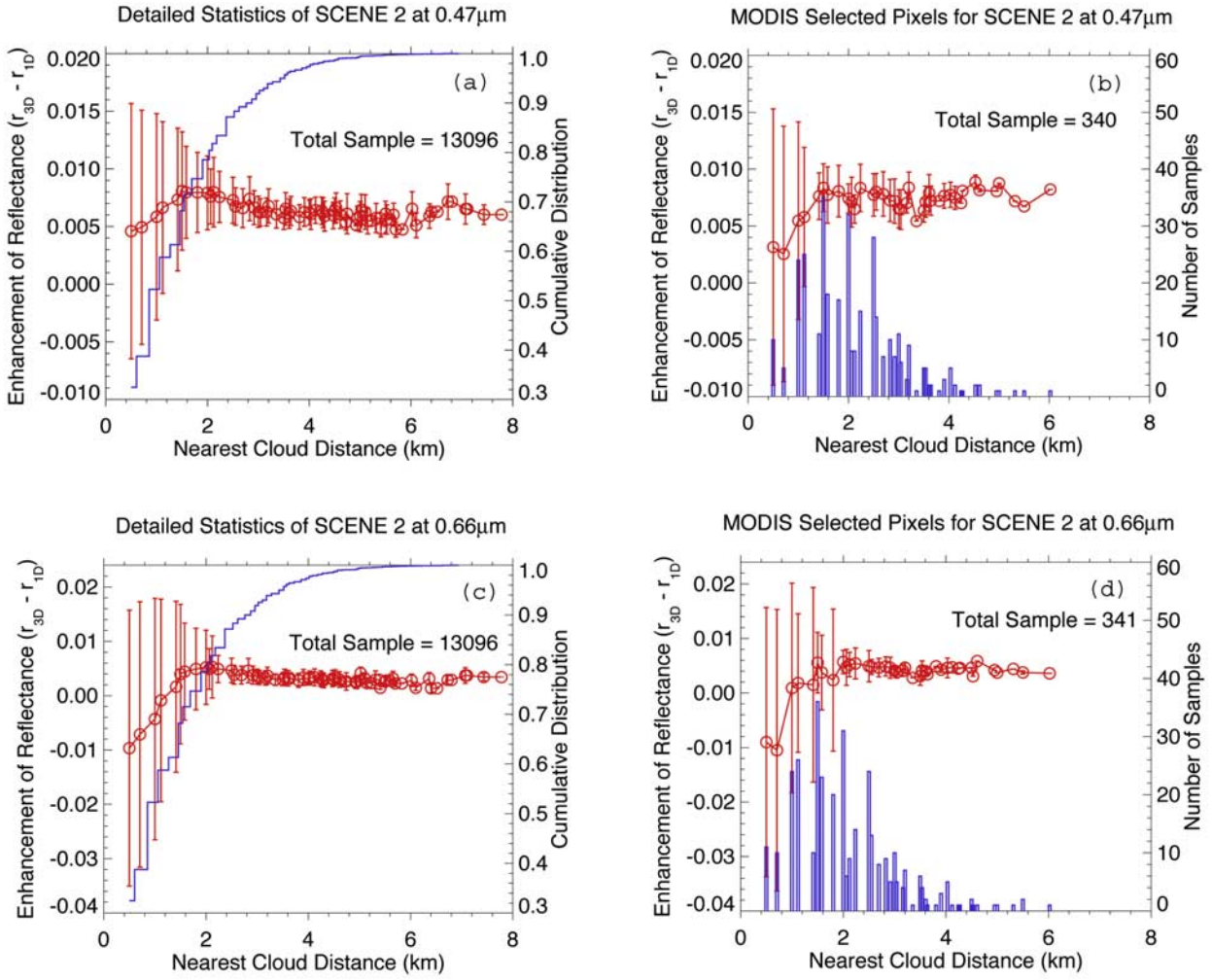

Figure 9. Average enhancement (circles, left scale) and standard deviation (vertical brackets) for clear pixels as a function of the nearest cloud distance. Cumulative and sample distributions of clear pixels as a function of the nearest cloud distance (right scale) for scene 1. Results are presented in Figures 9a and 9c for all noncloudy pixels at wavelengths 0.47 and 0.66 μm, respectively. Results for MODIS-selected pixels are presented in Figures 9b and 9d, respectively.

[32] The enhancement (or reduction) of the reflected radiation from shadowed pixels of scene 2 behaves differently from that in scene 1 at 0.47 μm. In scene 1, the enhancement of shadowed pixels is small but positive almost everywhere. In scene 2, the 3-D cloud effects reduce the reflectance over shadowed pixels, resulting in a negative enhancement or reduction. The shadowing reduction of reflectance is primarily associated with a brighter surface in scene 2. With the average surface albedo $\sim$0.01 in scene 1 versus $\sim$0.04 in scene 2, the surface in scene 1 is much darker than that in scene 2 at 0.47 μm.

[33] The distributions of the enhancement of reflectance for the two wavelengths and populations of all noncloudy pixels and those selected by MODIS aerosol retrieval algorithm are presented as a function of the nearest cloud distance (Figure 9). For all noncloudy pixels (Figures 9a and 9c), the enhancement at the two wavelengths shows a similar distribution as a function of nearest cloud distance. Large variability associated with the reduction over shadowed pixels and strong enhancement in front of the sunlit side of clouds is seen within $\sim$1.5 km of cloud edges. A wider cloud neighboring area compared to scene 1 is primarily due to a larger solar zenith angle of $\sim$40° in scene 2 compared to a smaller solar zenith angle of $\sim$30° in scene 1. Similar to scene 1, the variability of the enhancement for 0.66 μm in the cloud neighboring area (0.5–1.5 km) is twice as large as that for 0.47 μm (Figures 9a and 9c). The variability drops quickly in the first couple of kilometers from clouds. The average enhancement increases reaching a maximum at a distance 1.5 km away from cloud edges, then decreases gradually to asymptotic value of $\sim$0.006 at 0.47 μm and $\sim$0.003 at 0.66 μm at a distance about 3 km away from cloud edges. The enhancement of 0.006 and 0.003 can be translated to be an overestimate of the aerosol optical thickness of 0.06 and 0.03 if 3-D aerosol-cloud radiative interaction is ignored. Compared to the true aerosol optical thickness of 0.07 at 0.47 μm and 0.05 at 0.66 μm, 1-D approximation over-

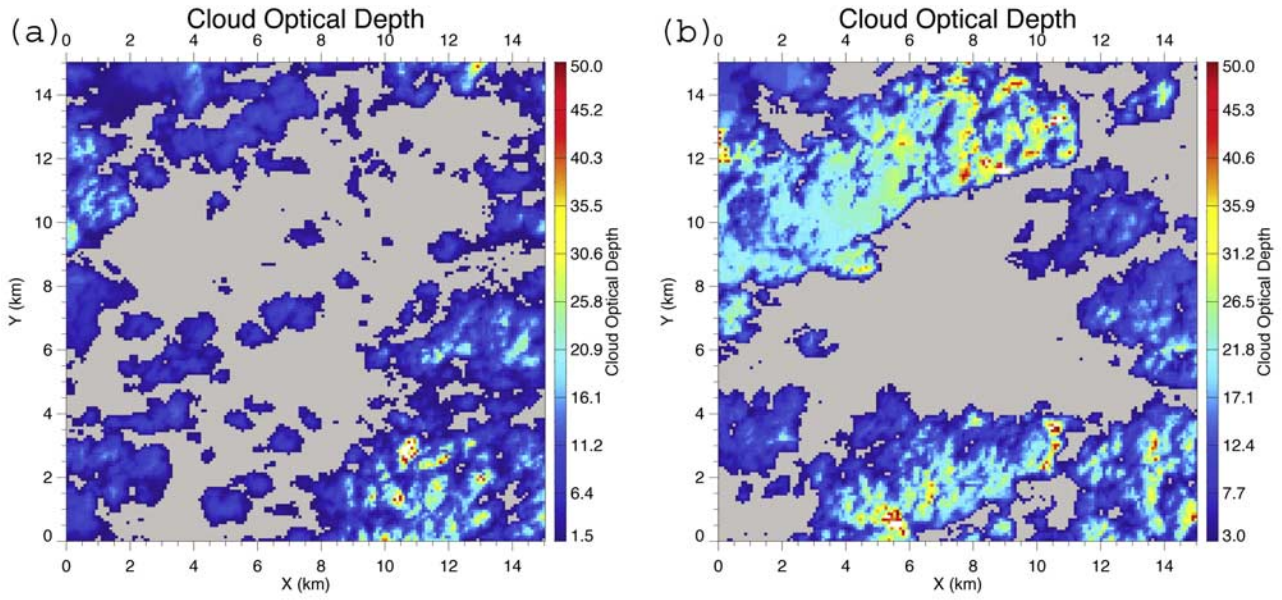

Figure 10. Cloud optical depth retrieved from an ASTER image collocated with scene 1. Shown are two subsets of the image both at 90-m resolution designated in Figure 2a as the two boxes outlined in black (a) for the upper box and (b) for the lower box shown in Figure 2a. The averages of cloud optical depth and standard deviations are (a) τ (thin clouds) $\sim$7 and σ (thin clouds) $\sim$6 and (b) τ (thick clouds) $\sim$14 and σ (thick clouds) $\sim$8. The cloud cover is $\sim$51 and $\sim$59% for Figures 10a and 10b, respectively.

estimates aerosol optical thickness by 86 and 60% at the two wavelengths, respectively.

[34] The distributions of the enhancement for pixels selected by MODIS aerosol retrieval algorithm are illustrated in Figures 9b and 9d. With more samples for the selected pixels, the distributions of the average enhancement and variability for the subset resemble those of the larger population of all noncloudy pixels (Figures 9a and 9c). However, there is a distinctive difference between the distributions for MODIS-selected pixels and their counterparts for overall noncloudy pixels. The distribution of the enhancement for the selected pixels reaches asymptotic value at a distance about 2 km away from cloud edges, rather than 3 km for overall noncloudy pixels. For the selected pixels, the asymptotic enhancement is 0.0075 and 0.0041 for the wavelength at 0.47 and 0.66 μm, respectively. Compared with the asymptotic enhancements of 0.006 and 0.0029 for the same wavelength, we found that the average enhancement for MODIS-selected pixels is about 0.0015 and 0.0012 larger than that for the overall noncloudy pixels. Again, the pixel selection process in the MODIS aerosol algorithm does not eliminate the significant enhancement of reflectance by 3-D effects.

[35] The overall population of clear pixels decreases away from cloud edges at a slower rate compared to scene 1. At a distance 3 km away from cloud edges, where the enhancement reaches asymptotic values, there are still about 10% of clear pixels left. At a distance 3.5 km, the clear pixel population drops to 5%. At a distance beyond 4.6 km from cloud edges, only 1% of clear pixels are left. It is also interesting to note that even at a distance about 6–8 km away from clouds, the enhancement does not vanish. Thus, under any circumstances, asymptotic enhancement of reflectance in clear regions of a cloudy atmosphere is very large, producing a biased aerosol retrieval from the 1-D approximation.

5. 3-D Cloud Effects at 90-m Resolutions

[36] As demonstrated above, spatial resolution is important when the scale of true variation is unresolved by the instrument. Examples of MODIS unresolved features are the size of cloud shadows and clouds smaller than 0.5 km in size. Cloud optical depth and cloud structure also vary in space. Distributions of the enhancement for scene 1 and scene 2 in section 4 describe the statistics for the whole image at 0.5-km MODIS resolution. To better understand the cloud effects on reflectance in nearby clear regions, we have to study 3-D radiative transfer at small scales unresolved by MODIS.

[37] In this study, the radiance at 0.66 μm from a simultaneous ASTER image is used to retrieve cloud optical thickness. The original 15-m resolution ASTER image is aggregated to the 90-m resolution image. Cloud optical depth fields retrieved from ASTER for the two subimages of MODIS highlighted in Figure 2a are presented in Figure 10. There are three features to mention. First, clouds in the lower subimage are optically thick compared to those in the upper subimage. The average cloud optical depth ($\tau \sim 14$) in the thick cloud field is twice as large as that ($\tau \sim 7$) in the optically thin cloud field. Second, the difference in cloud coverage is not dramatic between the two fields with $\sim$59 and $\sim$51% for the optically thick clouds and the thin clouds, respectively. Third is that the small puffy cumuli not identified in the MODIS cloud optical depth product are now resolved by ASTER.

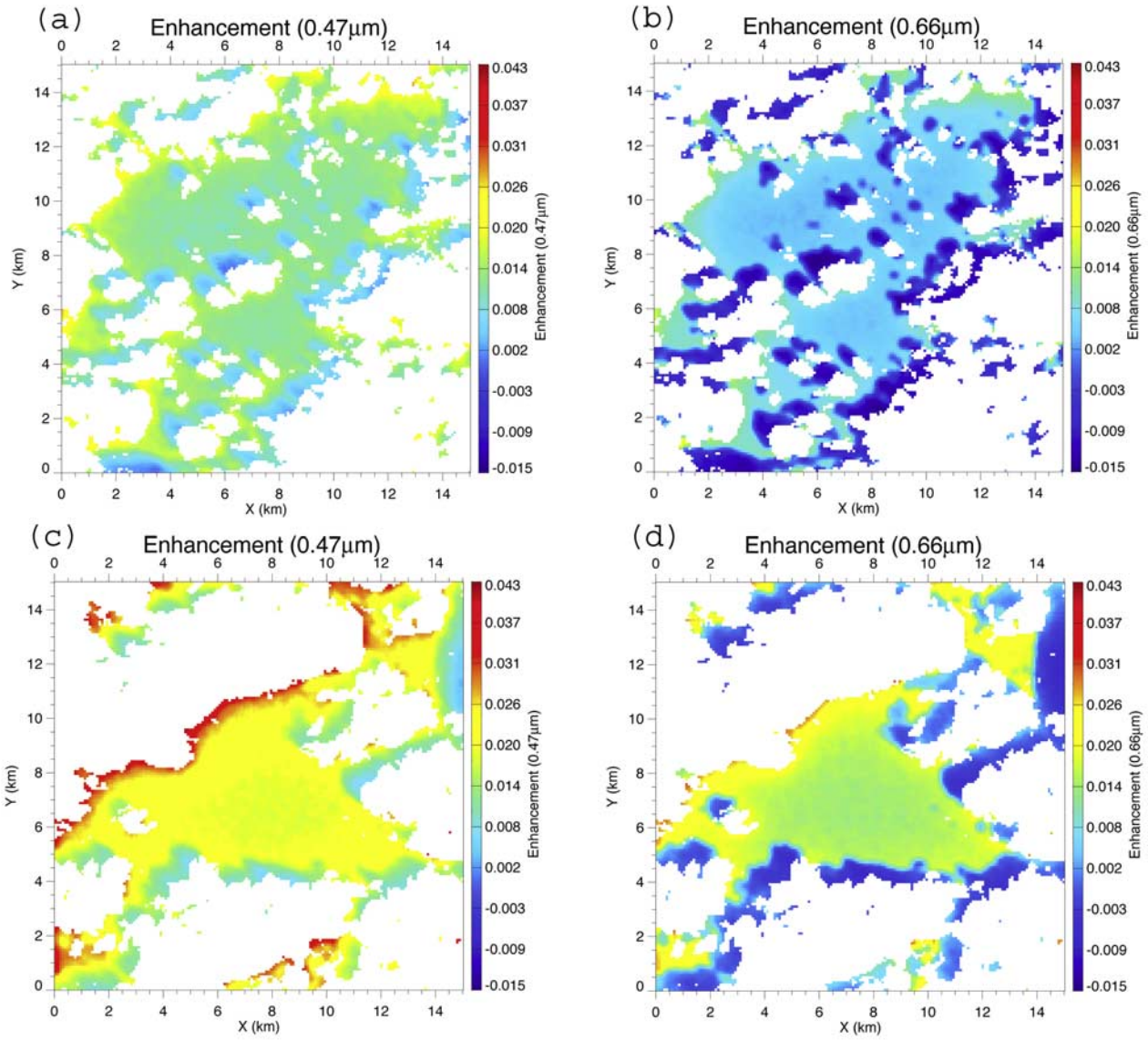

Figure 11. Enhancement of reflected solar radiation due to 3-D effects for clear regions in optically thin (upper panel) and thick cumulus (lower panel) for wavelengths at 0.47 μm (left) and 0.66 μm (right) at 90-m resolution. Cloud pixels are masked as white. For optically thin cloud field, $\overline{\Delta r}_{0.47\,\mu m}$ = 0.012 ($\sigma_{0.47\,\mu m}$ = 0.004) and $\overline{\Delta r}_{0.66\,\mu m}$ = 0.0018 ($\sigma_{0.66\,\mu m}$ = 0.007). For optically thick cloud field, $\overline{\Delta r}_{0.47\,\mu m}$ = 0.019 ($\sigma_{0.47\,\mu m}$ = 0.006) and $\overline{\Delta r}_{0.66\,\mu m}$ = 0.01 ($\sigma_{0.66\,\mu m}$ = 0.009). Asymptotic enhancement values that better characterize the 3-D effects are presented in Figure 12.

[38] The same amount of aerosols for the scene 1 study and the same average surface albedo are used in computing 3-D radiation fields for both subimages for the pair of wavelengths. The results are presented in Figure 11 for optically thin (upper panel) and thick (lower panel) cloud fields for the two wavelengths. Similar to the coarse resolution image, except for shadowed pixels at 0.66 μm, clouds enhance the reflectance almost everywhere in clear regions for both wavelengths. Small positive enhancement of reflectance over shadowed pixels at 0.47 μm is primarily due to the very low surface albedo as explained earlier.

[39] Near cloud edges, the enhancement of shadowed and sunlit sides is not uniformly distributed. It is clear from those images that the impact due to 3-D clouds does indeed depend on the resolution. Small clouds and their shadows are evidently unresolvable by MODIS with 0.5-km resolution. Large variability of the enhancement near cloud edges in the MODIS resolution of 0.5 km (see Figures 6 and 7) can be explained by the nonuniform variability at a smaller scale.

[40] The enhancement clearly depends on the optical depth of the nearby cloud field as well as wavelength. Similar to the coarse resolution, clouds have stronger impact with less variability (the range and standard deviation) on the average enhancement of reflectance at the shorter wavelength compared to the longer wavelength for the same cloud field (Figure 11). It is interesting to note that, at 0.66 μm, the average enhancement is small (0.0018) with

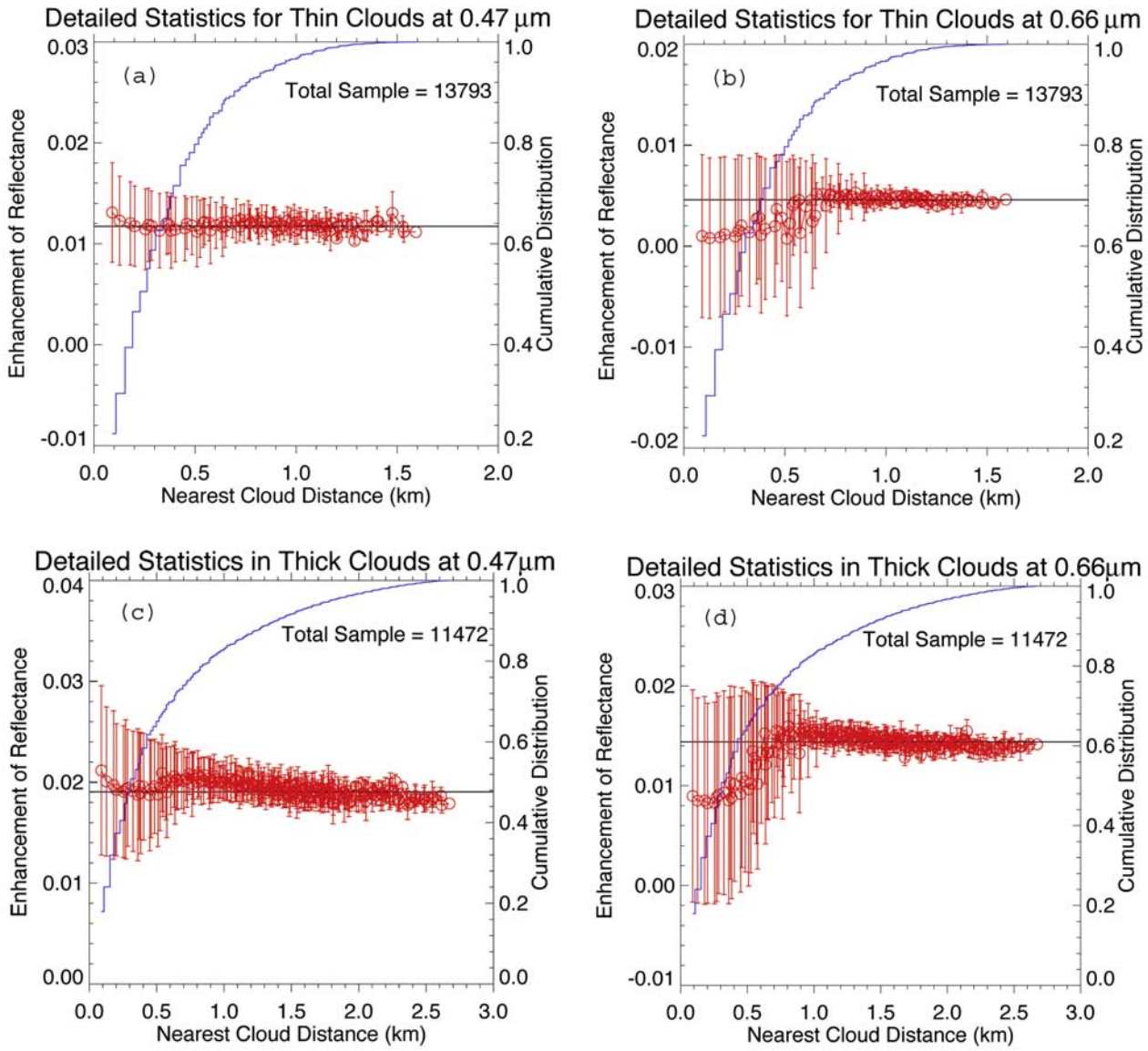

Figure 12. Similar to Figure 7 but for detailed statistics of the enhancement in the high-resolution images of Figure 11. The upper panels show the enhancement as a function of cloud distance and cumulative distribution for the image with optically thin clouds. The lower panels show the same for the image with thicker cloud. The left panels are for 0.47 μm and the right for 0.66 μm. The asymptotic values of the enhancement are $\Delta r_{0.47\ \mu m}$ (thin cloud) = 0.012, $\Delta r_{0.66\ \mu m}$ (thin cloud) = 0.0046; and $\Delta r_{0.47\ \mu m}$ (thick cloud) = 0.019, $\Delta r_{0.66\ \mu m}$ (thick cloud) = 0.014.

a large standard deviation of 0.007 in the optically thin cloud field. It is seen that the average enhancement increases by 50% and 5 times from optically thin clouds to optically thick clouds for wavelengths 0.47 and 0.66 μm, respectively.

[41] Distributions of enhancement and associated clear populations are presented in Figure 12. It is evident that enhancement has a large variability within the first 1 km from cloud edges, and reaches asymptotic values beyond 1 km. For the same reason as in the coarse resolution, the large variability near cloud edges is primarily due to the strong diffuse enhancing in front of the sunlit side of clouds and less enhancement or even reduction of shadowing effects. The relatively brighter surface at 0.66 μm compared with that at 0.47 μm is the cause of larger variability, even negative enhancement at the longer wavelength (see the standard deviations in the cloud neighboring region in Figure 12).

[42] Away from the extremes of 3-D impacts in the cloud neighboring region, the asymptotic values can be used to estimate 3-D cloud-induced enhancement of reflectance. Again, the asymptotic values depend on wavelength as well as optical depth of nearby cloud fields. For the optically thin clouds, the asymptotic values of the enhancement are 0.012

and 0.0046 for wavelengths 0.47 and 0.66 μm, respectively (Figures 12a and 12b). For the optically thick cloud field, the asymptotic values of the enhancement are 0.019 and 0.014 for 0.47 and 0.66 μm, respectively (Figures 12c and 12d). Since the true aerosol optical thickness is 0.2 and 0.1 for the two wavelengths, the 1-D approximation will overestimate aerosol optical thickness by $\sim$0.12 for 0.47 μm and $\sim$0.05 for 0.66 μm in the optically thin cloud field, about 50% larger than the true values. In the thick cloud field, ignoring 3-D aerosol-cloud radiative effects will lead to overestimates of aerosol optical thickness of about $\sim$0.2 for 0.47 μm and $\sim$0.14 for 0.66 μm. The systematic bias errors for thick clouds are $\sim$100 and $\sim$140% for the two wavelengths, respectively.

6. Summary and Discussions

[43] Two MODIS and ASTER collocated images of cumulus clouds are analyzed to study 3-D cloud-aerosol radiative interaction and its impact on aerosol retrievals. Our studies show that 3-D clouds enhance reflectance almost everywhere in clear pixels in cumulus fields except for shadowed pixels. The major factors that determine the magnitude of the enhancement are (1) the distance between the clear pixel and surrounding clouds: farther away from the clouds, the less the variability and the enhancement; (2) optical properties of surrounding clouds: the thicker the clouds, the larger the enhancement; (3) the wavelength considered: the shorter the wavelength, the larger the enhancement; (4) surface albedo: the larger the surface albedo, the larger the enhancement.

[44] By visually examining pixels selected for MODIS aerosol retrievals with collocated high-resolution ASTER images, we did not find evidence of cloud contamination for those selected pixels. This means that none of those pixels selected for the aerosol retrieval coincided with a cloud as identified with the high-resolution ASTER. We found that both the observed reflectance and 3-D clouds-induced enhancement have a slightly decreasing wavelength-dependent trend with the distance from the nearest cloud edge in scene 1. Since the surface is dark and homogeneous at the two wavelengths and there is no cloud contamination for those selected pixels, wavelength-dependent decreasing trends are likely due to 3-D cloud effects. We found that the shadowing effects are stronger at 0.66 μm compared to wavelength at 0.47 μm. We also found that the majority of clear pixels are within about 2 km away from cloud edges.

[45] Away from cloud edges where extreme situations of the 3-D radiative effects occur, the asymptotic enhancement provides an estimate of 3-D effects on both the radiation field and on aerosol retrievals from that field. For aerosol optical thickness of 0.2 at 0.47 μm in the "polluted" scene at 0.5-km resolution, we found that the overestimation of aerosol optical thickness will be about +0.1 (absolute) or +50% (relative) using a 1-D retrieval, which is about the same as that in the optically thin cloud field in the 90-m study. This bias error almost doubles in the thick cloud field. At the longer wavelength of 0.66 μm, the 1-D approximation leads to a less but still appreciably large systematic bias error (+40% in optically thin cloud field and+140% in optically thick cloud field) in aerosol optical thickness retrieval.

[46] 3-D cloud-induced enhancement of reflectance in the "pristine" scene is smaller compared to that in the "polluted" scene. But the asymptotic enhancement does not vanish even at a distance 6$\sim$8 km away from clouds. The bias error is about +85 and +60% of the ambient aerosol amount for wavelength 0.47 and 0.66 μm, respectively. We examined the enhancement for MODIS-selected pixels [for details, see *Remer et al.*, 2005] for the two scenes. We found that the enhancement of MODIS-selected pixels has similar magnitude to or even slightly larger ($\sim$0.001–0.002) than the enhancement determined from all noncloudy pixels for both scenes.

[47] One should note that the bias errors for "pristine" scene or "polluted" scene at 0.66 μm are close to the upper bound of expected uncertainty of MODIS aerosol retrieval of $\pm 0.05 \pm 0.15\tau$ over land [*Remer et al.*, 2005]. Our analysis indicates that the radiative effect of 3-D clouds is a potential source of error in long-term MODIS aerosol statistics. Combining the analyses of scene 1, scene 2, and optically thin and thick cloud fields, we conclude that the 3-D cloud-induced bias error from the 1-D retrieval in this study ranges from 50 to 140%.

[48] The results in this study are based on two images. In the real atmosphere, cloud properties change from scene to scene. However, the two scenes analyzed here span a broad range of cloud optical properties found in typical broken cumulus fields. Scene 1 represents a situation of clear regions completely surrounded by cumulus. In scene 2, most clear pixels are on one half of the image with most cloudy pixels on the other half. Particularly, the detailed studies at 90 m provide the range of the 3-D cloud-induced enhancement of reflectance for optically thin and thick clouds. The surface albedo differs from scene 1 to scene 2. The surface of scene 1 is dark and homogeneous. The surface of scene 2 is brighter and more variable compared to scene 1. Aerosol loadings and surface properties are also different for the two images. We expect the range of enhancement of aerosol optical thickness retrievals (50 to 140%) found in this study to apply in most situations of broken cumulus.

[49] Finally, we conclude that 3-D aerosol-cloud radiative interaction enhances extensively the reflectance in clear regions around broken clouds. The 3-D cloud-induced enhancement of reflectance depends on optical properties of nearby clouds as well as wavelength. Radiative effects of 3-D clouds are important in understanding of aerosol indirect effects on climate from satellite observations. Thus one should be cautious in applying the 1-D approximation to compute clear-sky solar radiation in cumulus fields or using aerosol products derived from the 1-D approximation in aerosol indirect effect research.

[50] **Acknowledgments.** This research was supported in part by the NASA's Radiation Program (under grants 622-42-57-20 and 621-30-86-20) and in part by the Office of Science (BER), U.S. Department of Energy (interagency agreement DE-AI02-95ER61961), as part of the ARM program.

References

Ackerman, S. A., K. I. Strabala, W. P. Menzel, R. A. Frey, C. C. Moeller, and L. E. Gumley (1998), Discriminating clear sky from clouds with MODIS, *J. Geophys. Res.*, *103*, 32,141–32,157.

Andreae, M. O., D. Rosenfeld, P. Artaxo, A. A. Costa, G. P. Frank, K. M. Longo, and M. A. F. Silva-Dias (2004), Smoking Rain Clouds over the Amazon, *Science*, *303*, 1337–1342, doi:10.1126/science.1092779.

Cahalan, R. F., L. Oreopoulos, G. Wen, A. Marshak, S. C. Tsay, and T. P. DeFelice (2001), Cloud characterization and clear sky correction from Landsat 7, *Remote Sens. Environ.*, *78*, 83–98.

Cahalan, R. F., et al. (2005), The International Intercomparison of 3D Radiation Codes (I3RC): Bringing together the most advanced radiative transfer tools for cloudy atmospheres, *Bull. Am. Meteorol. Soc.*, *86*(9), 1275–1293.

Chambers, L. H., B. A. Wielicki, and K. F. Evans (1997), Accuracy of the independent pixel approximation for satellite estimates of oceanic boundary layer cloud optical depth, *J. Geophys. Res.*, *102*, 1779–1794.

Coakley, J. A., Jr., R. L. Bernstein, and P. A. Durkee (1987), Effect of ship-track effluents on cloud reflectivity, *Science*, *237*, 1020–1022.

Feingold, G. (2003), Modeling of the first indirect effects: Analysis of measurement requirements, *Geophys. Res. Lett.*, *30*(19), 1997, doi:10.1029/2003GL017967.

Han, Q., W. Rossow, and A. Lacis (1994), Near-global survey of effective droplet radii in liquid water cloud using ISCCP data, *J. Clim.*, *7*, 465–497.

Hansen, J. (1971), Multiple scattering of polarized light in planetary atmospheres: Part II. Sunlight reflected by terrestrial water clouds, *J. Atmos. Sci.*, *28*, 1400–1426.

Holben, B. N., et al. (1998), AERONET - A federated instrument network and data archive for aerosol characterization, *Remote. Sens. Environ.*, *66*, 1–16.

Horváth, A., and R. Davies (2004), Anisotropy of water cloud reflectance: A comparison of measurements and 1D theory, *Geophys. Res. Lett.*, *31*, L01102, doi:10.1029/2003GL018386.

Iwabuchi, H., and T. Hayasaka (2003), A multi-spectral non-local method for retrieval of boundary layer cloud properties from optical remote sensing data, *Remote Sens. Environ.*, *88*, 294–308.

Intergovernmental Panel on Climate Change (2001), Climate Change 2001: The Scientific Basis. Contribution of Working Group I to the Third Assessment Report of the Intergovernmental Panel on Climate Change, edited by J. T. Houghton, Y. Ding, D. J. Griggs, M. Noguer, P. J. van der Linden, X. Dai, K. Maskell, and C. A. Johnson, 881 pp., Cambridge Univ. Press, New York.

Joseph, J. H., and R. F. Cahalan (1990), Nearest neighbor spacing of fair weather cumulus clouds, *J. Appl. Meteorol.*, *29*, 793–805.

Kaufman, Y., and R. Fraser (1997), The effect of smoke particles on clouds and climate forcing, *Science*, *277*, 1636–1639.

Kaufman, Y., et al. (2005), A critical examination of the residual cloud contamination and diurnal sampling effects on MODIS estimates of aerosol over ocean, *IEEE Trans. Geosci. Remote Sens.*, *43*, 2886–2897.

Kaufman, Y. J., and I. Koren (2006), Smoke and pollution aerosol effect on cloud cover, *Science*, *313*, 655–658, doi:10.1126/science.1126232.

Kobayashi, T., K. Masuda, M. Sasaki, and J. Mueller (2000), Monte Carlo simulations of enhanced visible radiance in clear-air satellite fields of view near clouds, *J. Geophys. Res.*, *105*(D21), 26,569–26,576.

Lane, D. E., K. Goris, and R. C. J. Somerville (2002), Radiative transfer through broken clouds: Observations and model validation, *J. Clim.*, *15*, 2921–2933.

Marshak, A., and A. Davis (2005), *3D Radiative Transfer in Cloudy Atmospheres*, Springer, New York.

Marshak, A., S. Platnick, T. Várnai, G. Wen, and R. F. Cahalan (2006), Impact of 3D radiative effects on satellite retrievals of cloud droplet sizes, *J. Geophys. Res.*, *111*, DO9207, doi:10.1029/2005JD006686.

Martins, J. V., D. Tanre, L. A. Remer, Y. J. Kaufman, S. Mattoo, and R. Levy (2002), MODIS cloud screening for remote sensing of aerosol over oceans using spatial variability, *Geophys. Res. Lett.*, *29*(12), 8009, doi:10.1029/2001GL013252.

Moody, E. G., M. D. King, S. Platnick, C. B. Schaaf, and F. Gao (2005), Spatially complete global spectral surface albedos: Value-added datasets derived from Terra MODIS land products, *IEEE Trans. Geosci. Remote Sens.*, *43*, 144–158.

Nikolaeva, O. V., L. P. Bass, T. A. Germogenova, A. A. Kokhanovisky, V. S. Kuznetsov, and B. Mayer (2005), The influence of neighboring clouds on the clear sky reflectance with the 3-D transport code RADUGA, *J. Quant. Spectrosc. Radiat. Transfer*, *94*, 405–424.

Platnick, S., P. A. Durkee, K. Nielson, J. P. Taylor, S. C. Tsay, M. D. King, R. J. Ferek, P. V. Hobbs, and J. W. Rottman (2000), The role of background cloud microphysics in the radiative formation of ship tracks, *J. Atmos. Sci.*, *57*, 2607–2624.

Platnick, S., M. King, S. Ackerman, W. P. Menzel, B. Baum, J. C. Riedi, and R. A. Frey (2003), The MODIS cloud products: algorithms and examples from Terra, *IEEE Trans. Geosci. Remote Sens.*, *41*, 459–473.

Reid, J., S. Hobbs, P. V. Ferek, R. J. Blake, D. R. Martins, J. V. Dunlap, and M. R. Liousse (1998), Physical, chemical and optical properties of regional hazes dominated by smoke in Brazil, *J. Geophys. Res.*, *103*, 32,059–32,080.

Remer, L., et al. (2005), The MODIS aerosol algorithm, products, and validation, *J. Atmos. Sci.*, *62*, 947–973, special section.

Twomey, S. (1977), The influence of pollution on the shortwave albedo of clouds, *J. Atmos. Sci.*, *34*, 1149–1152.

Várnai, T., and A. Marshak (2002), Observations of three-dimensional radiative effects that influence MODIS cloud optical thickness retrievals, *J. Atmos. Sci.*, *59*, 1607–1618.

Yamaguchi, Y., A. B. Kahle, H. Tsu, T. Kawakami, and M. Pniel (1998), Overview of Advanced Spaceborne Thermal Emission and Reflection Radiometer (ASTER), *IEEE Trans. Geosci. Remote Sensing*, *36*, 1062–1071.

Wen, G., S.-C. Tsay, R. F. Cahalan, and L. Oreopoulos (1999), Path radiance technique for retrieving aerosol optical thickness over land, *J. Geophys. Res.*, *104*, 31,321–31,332.

Wen, G., R. F. Cahalan, S.-C. Tsay, and L. Oreopoulos (2001), Impact of cumulus cloud spacing on Landsat atmospheric correction and aerosol retrieval, *J. Geophys. Res.*, *106*, 12,129–12,138.

Wen, G., A. Marshak, and R. F. Cahalan (2006), Impact of 3D clouds on clear sky reflectance and aerosol retrieval in a biomass burning region of Brazil, *IEEE Geo. Rem. Sens. Lett.*, *3*, 169–172.

R. F. Cahalan, A. Marshak, L. A. Remer, and G. Wen, NASA Goddard Space Flight Center, Code 613.2, Greenbelt, MD 20771, USA. (wen@climate.gsfc.nasa.gov)

R. G. Kleidman, Science Systems and Applications, Inc., Lanham, MD, USA.